HHS Public Access

Author manuscript

Sci Transl Med. Author manuscript; available in PMC 2022 June 27.

Published in final edited form as:

Sci Transl Med. 2019 June 12; 11(496): . doi:10.1126/scitranslmed.aat5857.

In vivo liquid biopsy using Cytophone platform for photoacoustic detection of circulating tumor cells in patients with melanoma

Ekaterina I. Galanzha[1,2],

Yulian A. Menyaev[1],

Aayire C. Yadem[1,3],

Mustafa Sarimollaoglu[1,2],

Mazen A. Juratli[1,4],

Dmitry A. Nedosekin[1],

Stephen R. Foster[5],

Azemat Jamshidi-Parsian[6],

Eric R. Siegel[7],

Issam Makhoul[8],

Laura F. Hutchins[8],

James Y. Suen[9],

Vladimir P. Zharov[1,2,9,*]

[1]Arkansas Nanomedicine Center, University of Arkansas for Medical Sciences, 4301 West Markham Street, Little Rock, AR 72205, USA.

[2]Laboratory of Biomedical Photoacoustics, Saratov State University, 83 Astrakhanskaya Street, Saratov, 410012, Russia.

[3]Department of Applied Science (Physics), University of Arkansas at Little Rock, 2801 South University Avenue, Little Rock, AR 72204, USA.

[4]Department of General and Visceral Surgery, University Hospital of Frankfurt, Theodor-Stern-Kai 7, 60590 Frankfurt am Main, Germany.

[5]Institute of Aging, University of Arkansas for Medical Sciences, 4301 West Markham Street, Little Rock, AR 72205, USA.

[*]Corresponding author. zharovvladimirp@uams.edu.

Author contributions: E.I.G. and V.P.Z. designed the study and wrote the paper; Y.A.M. and A.C.Y. performed experiments in vivo; M.A.J., D.A.N., S.R.F., and A.J.-P. performed experiments in vitro; M.S. developed software for PAFC; E.R.S. provided statistical analysis; and I.M., L.F.H., and J.Y.S. supported human-participant involvement.

Competing interests: V.P.Z. and E.I.G. and the University of Arkansas for Medical Sciences (UAMS) have a financial interest in the technology discussed in this publication. V.P.Z. and J.Y.S. have a financial interest in CytoAstra, LLC, which holds a license for the use of the technology discussed in this publication. These financial interests have been reviewed and approved in accordance with the UAMS conflict of interest policies. All other authors declare that they have no competing interests.

Data and materials availability: All data associated with this study are present in the paper or the Supplementary Materials.

SUPPLEMENTARY MATERIALS

stm.sciencemag.org/cgi/content/full/11/496/eaat5857/DC1

[6]Department of Radiation Oncology, University of Arkansas for Medical Sciences, 4301 West Markham Street, Little Rock, AR 72205, USA.

[7]Department of Biostatistics, University of Arkansas for Medical Sciences, 4301 West Markham Street, Little Rock, AR 72205, USA.

[8]Division of Hematology Oncology, University of Arkansas for Medical Sciences, 4301 West Markham Street, Little Rock, AR 72205, USA.

[9]Department of Otolaryngology–Head and Neck Surgery, University of Arkansas for Medical Sciences, 4301 West Markham Street, Little Rock, AR 72205, USA.

Abstract

Most cancer deaths arise from metastases as a result of circulating tumor cells (CTCs) spreading from the primary tumor to vital organs. Despite progress in cancer prognosis, the role of CTCs in early disease diagnosis is unclear because of the low sensitivity of CTC assays. We demonstrate the high sensitivity of the Cytophone technology using an in vivo photoacoustic flow cytometry platform with a high pulse rate laser and focused ultrasound transducers for label-free detection of melanin-bearing CTCs in patients with melanoma. The transcutaneous delivery of laser pulses via intact skin to a blood vessel results in the generation of acoustic waves from CTCs, which are amplified by vapor nanobubbles around intrinsic melanin nanoclusters. The time-resolved detection of acoustic waves using fast signal processing algorithms makes photoacoustic data tolerant to skin pigmentation and motion. No CTC-associated signals within established thresholds were identified in 19 healthy volunteers, but 27 of 28 patients with melanoma displayed signals consistent with single, clustered, and likely rolling CTCs. The detection limit ranged down to 1 CTC/liter of blood, which is ~1000 times better than in preexisting assays. The Cytophone could detect individual CTCs at a concentration of ≥1 CTC/ml in 20 s and could also identify clots and CTC-clot emboli. The in vivo results were verified with six ex vivo methods. These data suggest the potential of in vivo blood testing with the Cytophone for early melanoma screening, assessment of disease recurrence, and monitoring of the physical destruction of CTCs through real-time CTC counting.

INTRODUCTION

Circulating tumor cells (CTCs) are cancer cells shed by either a primary tumor or metastasis in the blood network and lymphatics (1). Since the first observation of CTCs in a cancer patient’s blood (2), many studies demonstrated the potential of CTCs as a prognostic marker of metastasis and responses to therapies (3-9). However, the role of CTCs as an early disease marker is still unclear because existing CTC assays (including CellSearch, microfluidic chips, cell-size filtration, and negative selection among many others) are burdened with low sensitivity at the level of 1 to 10 CTCs/ml (1, 4). This limitation is mostly attributed to the small volume of blood being sampled (a few milliliters), in which obviously no less than one CTC could be detected. Thus, these assays would fail to detect less than 10^3 to 10^4 CTCs in an adult’s entire blood volume (~5 liters). As a result, a difficult-to-treat metastasis can be established at the time of initial diagnosis. In addition, low marker expression [for example, the epithelial surface cell adhesion molecule (EpCAM) is absent in melanoma], along with

multiple sample-processing steps including labeling, immunomagnetic capture, isolation, and washing, can result in additional CTC loss (1). The examination of larger blood volumes can improve the detection threshold (CTCs were found in 13 and 47% of patients using 7.5 and 30 ml of blood samples, respectively); nevertheless, collection of blood volumes above 50 ml is clinically limited (4). The capturing of CTCs by insertion of functionalized gold wire directly into blood vessels using the CellCollector device with further analysis of captured EpCAM-positive cells ex vivo showed an increase in diagnosis sensitivity (5, 6). A total of 58% of patients with lung cancer were positive for ≥1 CTC compared to only 27% using the U.S. Food and Drug Administration–cleared CellSearch system (5). Nevertheless, invasive extraction of blood or wire from the patients may cause changes in CTC signaling or functional state, as well as artifacts such as clotting and CTC aggregation. In general, inconsistent results are increasingly reported among the various CTC assays, especially in the correlation between the presence of CTCs and survival rate (4). As a result, CTC assays are not yet recommended for broad use in cancer clinics.

The noninvasive assessment of large blood volumes is feasible with in vivo photoacoustic (PA) flow cytometry (PAFC) (7, 8) using the PA effect as a transformation of absorbed laser pulse energy into sound through thermoelastic expansion of light-heated objects. The PA effect was originally described by Bell (9) in 1860 as the principle behind the photophone, and has been used in gas analysis, spectroscopy, and imaging (10). Recently, PA medical devices have demonstrated their clinical potential for in vivo assessment of Crohn's disease status (11), imaging of breast cancer tumors (12), monitoring lymph node status (13), and control of blood oxygenation in jugular veins in the neck area (14). However, PA imaging can be too slow for detection of fast-moving CTCs, especially in large vessels, and the PAFC platform has been used in animal models only. Here, we present the application of PAFC for noninvasive, label-free detection of CTCs directly in the bloodstream of patients with melanoma using a Cytophone platform.

Over 1 million new melanoma cases are diagnosed each year, and one person dies of melanoma every hour in the United States. The most alarming aspect of this aggressive malignancy is its potential to metastasize at an early disease stage, and its incidence has been growing (15). Once melanoma has metastasized to distant organs, the average 5-year survival is 15 to 10%, whereas for patients with very early, nonmetastatic disease, 5-year survival rates are greater than 97% (15). The development of B-Raf proto-oncogene (BRAF) and MEK (the mitogen-activated protein kinase enzymes MEK1 and/or MEK2) inhibitors (for patients with mutations of the *BRAF* gene in their tumors) and immune checkpoint therapy with ipilimumab against cytotoxic T lymphocyte-associated antigen 4 (CTLA-4) and with pembrolizumab and nivolumab against programmed cell death protein 1 (PD-1) improved melanoma treatment (16-18). Nevertheless, after advanced therapy, some patients on these regimens can eventually relapse because cancer cells may find additional pathways to continue growing and spreading (19). Early detection of melanoma followed by immediate treatment is vital for reducing the risks of deadly metastasis.

In addition, thromboembolic events and, particularly, circulating blood clots (CBCs) that eventually block blood vessels in vital organs are the second leading cause of death among patients with cancer (20). In patients with melanoma, thromboembolic complications

occur after sentinel lymph node excision, isolated limb perfusion, implantation of a central venous catheter, or chemotherapy (6.5-fold increase in the risk of venous thromboembolism) (20-22). We have demonstrated PA detection of CBCs in large and deep animal vessels (23). Here, we show that Cytophone-based label-free detection of CTCs can also identify CBCs and CTC-CBC emboli in patients with melanoma in vivo.

RESULTS

Principle of Cytophone-based blood test

After multiple verifications in animal models (7, 8, 24, 25), we have applied a PAFC schematic with the transcutaneous delivery of laser pulses with widths of 0.8, 5, and 10 ns at a wavelength of 1060 nm and energy up to 240 μJ through intact skin to a vein with a diameter of 1.1 to 2.8 mm and a depth of 1 to 1.5 mm in the palm region of the human hand (Fig. 1 and figs. S1 and S2). Laser heating of light-absorbing hemoglobin (Hb) in red blood cells (RBCs) and melanin expressed in melanoma CTCs (fig. S3, A and B) caused thermoacoustic and nanobubble-based generation of acoustic waves (referred to as the PA signals) recorded with a small ultrasound transducer placed over the skin and displayed as the PA trace (Fig. 1D). PA signals from many RBCs in the detection volume created a trace baseline. When single or clustered melanoma CTCs with a high melanin absorption (Fig. 1C) pass through the detection volume, local absorption increases, resulting in sharp positive transient single or multiple PA peaks above blood background, respectively (Fig. 1D). When white CBCs, consisting of platelets, white blood cells (WBCs), and fibrin, with much lower absorption than the blood background, pass through the detection volume, the resulting decrease in local absorption produces a sharp negative PA peak. CTC-CBC aggregates, also called emboli, produce a pattern of positive and negative peaks (Fig. 1D). Because of light scattering in tissue resulting in laser beam blurring, the resolution of PAFC is determined by acoustic resolution of the focused cylindrical transducer of 65 ± 6 μm (Fig. 1B). The cylindrical transducer configuration allowed us to minimize the detection volume and hence maximize the signal-to-background ratio when simultaneously assessing all CTCs and CBCs in the blood vessel’s entire cross section.

In a preclinical study, PAFC parameters were optimized using large mouse blood vessels (24) similar in size (~1 mm), depth (1 to 2 mm), and flow velocity (4 to 7 cm/s) to veins in the human hand. With increased energy fluence, the PA signals from melanoma cells increase nonlinearly, in contrast to the linear increase seen with RBCs only (fig. S3C). This signal behavior is associated with laser-induced nanobubbles around overheated melanin clusters (fig. S3A) with high local absorption as a nonlinear signal amplifier with a gain in the range of 5 to 50. More homogeneously distributed Hb in RBCs produced no bubbles at the same laser energy (7, 25). Eventually, nanobubbles resulted in physical CTC destruction through a photomechanical mechanism (8) even during just one or a few laser pulses (fig. S3C). Comparison of PA signals at different laser pulse widths from melanoma cells and melanosomes revealed increasing signal amplitudes with decreasing pulse widths from 10 to 5 ns and then slight signal saturation with further width decrease to 0.8 ns (fig. S3D). This behavior is explained by appropriate matching of the subnanosecond pulses and melanin

nanoclusters (granules) with the sizes of 150 to 300 nm and larger (fig. S3, A and B) according to so-called thermal and acoustic confinements in PAFC (7).

The reproducibility of the PAFC systems over time was assessed by repeated PA signal measurements every day for a week from a vessel phantom with flowing blood and CTC phantoms (26). The fluctuation of the PA signal amplitudes was in the range of 19 to 26%, which is typical for PA techniques (27).

In vivo testing of healthy participants

Data from the first cohort of 10 healthy individuals were used to define the parameters of the PAFC (the laser energy and transducer sensitivity) and PAFC-related measurement procedures such as skin clearing (28) and positioning of the PA probe (consisting of the optical focusing tip and ultrasound transducer) on the participant's skin above the selected vein (fig. S1B). Standard ultrasound gel provided acoustic coupling between the transducer and the skin. The navigation of the transducer focal volume on the examined vein was controlled by optical and ultrasound imaging (Fig. 2A and fig. S1B). If any skin lesions, large hair, or other abnormalities were present, we avoided doing PA detection on the affected area by slightly changing the probe's position. The PA signal amplitudes from the selected veins were 1.5 ± 0.3 (SD) and 3.6 ± 0.8 times higher than the background signals from high- and low-pigmented skin, respectively. The time-resolved detection of PA signals came from the vein to the transducer with a width of 0.2 to 0.3 μs and a well-distinguished acoustic time delay (0.5 to 2 μs) compared to background PA signals from the pigmented skin layer (Fig. 2, B and C). This allowed us to completely eliminate the influence of skin background on the PAFC sensitivity. The quick (5 to 10 min) optical skin clearing with a combination of microdermabrasion and glycerol sonophoresis (28) provided a two- to threefold increase in PA signal amplitude from the vein through decreased light scattering in the superficial skin layer and consequent reduction of laser beam blurring. The volunteers reported no pain or skin property changes, and only an occasional warming sensation at the energy of 240 μJ at pulse rate of 10 kHz and linear beam size of 48 μm × 1250 μm. Decreasing the pulse rate to 1 to 2 kHz and beam size to 16 μm × 880 μm allowed us to use a relatively high energy of 100 μJ to 240 μJ on skin with no adverse effects such as the sensation of warmth.

Healthy volunteers were also used to test our ability to distinguish artifacts, determine the false positivity, and measure PA signals from vessels of different sizes and depth locations in each participant (table S1). The baseline of the PA trace is associated with blood background (Fig. 1D), which is proportional to the number of RBCs in the detection volume (23). The fluctuation of the baseline is determined by several factors such as a fluctuation of the RBC number (important for small vessels only), electronic noise, influence of scattered light, instability of the laser energy (typically 1 to 3%), acoustic environment noises, vibration, and hand movement (7, 23). Compared to PA signals from the vessels (Fig. 2B and fig. S4A), we tested the responses of PAFC to artificially induced hand motion, strong individual breathing, quick door closing, or vibrations (fig. S4, B to H). Under a typical vessel's parameters (flow velocity of 3 to 7 cm/s in a 1.3- to 2.8-mm vein), the expected lifetime of CTCs in the detection volume and, hence, the duration of transient sharp peaks in PA traces

ranged from 0.5 to 1.5 ms (see details below), whereas the duration of the non-CTC–related fluctuation baseline was longer (≥10 to 50 ms). Application of high-pass filtration together with signal averaging (Fig. 2, D and E) and then suppression of artifacts (24) provided a stable baseline over 1 hour (Fig. 2, F and G). Nevertheless, to reduce possible influence of hand movement due to strong tremor in a few participants, the hands of these particular patients were gently fixed in a customized holder (fig. S1C).

As a result, after postprocessing, no transient positive CTC-related PA signals above established blood background within established thresholds were identified in the volunteers (Fig. 2F). In particular, from one to two artifacts per person were identified in only six individuals, and they were easily excluded from further analysis. Only one unidentified artifact was observed in 1 subject among 19. These data suggest that, after artifact identification, CTC-related specificity of the PAFC can be estimated as 94.74%.

The PA signal amplitude was reproducible to within 31% when testing the same volunteer's vessels during the same day, which is in line with the phantom data above. The slightly larger signal fluctuations compared to the phantom could be explained by person-to-person variation of vessel diameters and the depth location.

In three other healthy participants with all physiological and blood parameters within the norms, we distinguished a few negative peaks (fig. S5). One of these three volunteered to take aspirin while periodically being measured by in vivo PAFC over a 6-week period. This participant's negative peaks disappeared after 3 weeks.

In vivo testing of patients with melanoma

We obtained PA traces from a training set of 18 patients with melanoma (see table S1 for gender, disease stage, and vessel parameters) where we defined the Cytophone's PAFC-related parameters. In particular, we tested software and laser parameters (for example, energies and pulse durations) for collecting PA signals from CTCs.

Having optimized the PAPC parameters for CTC detection in the training set, we fixed the parameters and tested them for performance on a validation set consisting of 10 new patients with melanoma (P19 to P28 in Table 1). We observed peaks exceeding blood background with the following patterns (Fig. 2H and fig. S6A): (i) positive single peaks with a width in the range of 0.5 to 1.5 ms associated with individual CTCs; (ii) positive peaks with relatively broad widths (3 to 5 ms) and complex shapes associated with CTC clusters; (iii) negative single peaks with different amplitudes and typical widths in the range of 20 to 50 ms associated with white platelet–rich CBCs; and (iv) combined positive and negative peaks associated with CTC-CBC emboli (Table 2). The PA signals from CTCs and CBCs had a specific shape (10-11, 23), duration, and time delay (Fig. 2, B and C) that allowed us to distinguish them easily from the artifacts of different origins (fig. S4, B to H).

The positive peak rate (number of peaks per time unit) and peak amplitude are associated with CTC concentration and content of melanin in each CTC, respectively. CTCs were unambiguously detected in 17 of 18 patients with melanoma in the training set (Table 1) and all 10 patients in the validation set, which likely suggests the absence of amelanotic

CTCs and high Cytophone sensitivity. In some patients, we observed many CTCs traveling closely together as a “CTC train,” which may indicate periodic release of groups of cancer cells from the tumor into the circulation. On the basis of the ability of PAFC to measure cell speed (7), we also identified slowly moving CTCs with the velocity of 0.4 to 1 cm/s in a flow with a velocity of 3 to 4 cm/s (also verified with ultrasound technique), which suggests that these CTCs are probably located close to the vessel wall or may even be rolling CTCs. For patients with a high CTC concentration resulting in frequent PA peaks, detection of the first CTC was achieved very quickly during the first 10 to 20 s at 1 CTC/ml. For patients with low CTC concentration, the monitoring process took from 15 to 60 min, thereby allowing us to examine 200 to 1000 ml of circulated blood, depending on blood velocity and vessel size (table S1). For example, during 60 min of monitoring a vein in patient P8, which had a diameter of ~3.0 mm and flow velocity of 4.12 cm/s, we were able to assess 954 ml of flowing blood, which allowed us to achieve an ultimate detection limit of ~1 CTC per 1 liter of blood. The concentration range of CTCs spanned more than three orders of magnitude, from 3 CTCs/ml down to 6 CTCs/liter. Only 8 (29%) of 28 patients with melanoma exceeded the ≥1 CTC/ml threshold needed for reliable detection by conventional assays. Although unambiguous CTC detection failed in one patient (P5; see Table 1), this patient did demonstrate a few low PA signal amplitudes slightly above the noise. Because this particular patient was intensively treated beforehand, this ambiguous result could reflect successful therapy.

In several patients (for example, P2 and P16), we periodically monitored the PA signals over the course of a day, using four 15-min sessions interspersed with break times of around 5 min in length. The reproducibility of CTC-associated peaks above blood background (Fig. 2G) was in the range of 25 to 55%. Besides instrumental reproducibility, this range can be associated with natural biological CTC fluctuation (7). However, we also observed the tendency of decreasing CTC counts over the course of the monitoring time (fig. S6B).

Testing blood samples using in vitro PAFC

PA data obtained in vivo were verified using six independent ex vivo assays (tables S2 to S6): (i) two in vitro PAFC setups with different schematics (Fig. 3A and fig. S7, A to G); (ii) conventional flow cytometry using a cocktail of two antibodies conjugated to fluorescein isothiocyanate (FITC) to target the melanoma markers chondroitin sulfate proteoglycan (MCSP) and CD146, mixed with phycoerythrin (PE)–conjugated antibody against CD45 receptor to identify WBCs; (iii) magnetic-activated cell sorting (MACS) using MCSP; (iv) quantitative reverse transcription-polymerase chain reaction (qRT-PCR) with seven melanoma markers (*ABCB5*, *MAGEA3*, *MCAM*, *MLANA*, *PAX3*, *TGFB2*, and *TYR*) together with the housekeeping gene *GAPDH*; (v) immunocytochemical staining using the HiDef Detection system and the Pan Melanoma antibody cocktail (HMB-45, MART-1, and tyrosinase; CBLPath Inc.); and (vi) integrated transmission (bright field), fluorescence, PA, and photothermal (PT) microscopy (7, 8). Because of the well-known limitations in the sensitivity of in vitro CTC assays (1, 5, 7), we increased the assay types to six to get multiple confirmations of the presence of CTCs in the patients with relatively high CTC concentrations (≥0.5 to 1 CTC/ml) assessable with these assays.

The first in vitro PAFC-based CTC assay was similar in technical parameters to the in vivo PAFC setup, in which the human hand was replaced by a vessel phantom consisting of a glass tube with circular cross section having an inner diameter of 0.8 mm (Fig. 3, A to C). The tube, a cylindrical transducer, and optical focusing tip were immersed in a tank with deionized water for acoustic coupling between the transducer and the tube. The typical volume of flowing blood samples was in the range of 1 to 6 ml in most studies and 40 ml in two selected experiments. In the second PAFC setup (fig. S7, A to D), we used higher laser energy, pulse rate, and smaller tube size (100 μm) to improve sensitivity and resolution.

We observed false-positive peaks in blood samples from healthy participants and even in deionized water using the tubes with sodium citrate and heparin (fig. S7, E and F) due to the high sensitivity of PAFC to small white and red (Hb-rich) clots even in stabilized blood, as well as some contaminants associated with light-absorbing crystals in sodium citrate, dark fragments of the tube caps formed during needle piercing, and flakes of polymer coating detached from the tube's outer surface (fig. S7G). Filtering the solution with a 0.22-μm acetate filter markedly decreased the number and amplitude of false-positive signals. EDTA tubes with sample stabilization in ice provided the best results (Fig. 3, D and E), with rare positive signals (identified as artifacts) in blood samples from healthy volunteers, which were used to establish the detection threshold (Fig. 3F and fig. S7E, top).

Using the blood shortly after collection in EDTA tubes, no transient positive PA signals were observed in the samples within an hour of blood collection from healthy volunteers within the established threshold (Fig. 3F and fig. S8B). In unprocessed whole blood samples from patients with melanoma, we observed CTC- and CBC-related PA-positive and small PA-negative peak (Fig. 3G; fig. S8, A, C, and D; and tables S2 and S3). Comparison of CTC detection rates in vivo and in vitro yielded a Spearman correlation coefficient of +0.570 (P = 0.0266). In addition, comparison of results determined in vivo and in vitro for 15 patients yielded two concordant results (13%) for CTCs detected, one concordant result (7%) for CTCs not detected, and twelve discordant results (Cohen's $\kappa \pm SE = 0.02 \pm 0.13$). However, calculated concentrations of CTCs in vitro were proportionally higher than in vivo. This discrepancy could be related to the in vitro use of a tube diameter smaller than typical in vivo vein diameters (0.8 mm versus 1.3 to 2.8 mm), higher energy fluence in vitro due to some uncertainty in vein depth, and optical tissue parameters preventing correct estimation of the laser light attenuation in tissue. The absence or low peak number in vitro in the samples from a few patients was explained by low CTC concentration (≤0.05 CTCs/ml), which is detectable in vivo but below the detection limit of PAFC in vitro due to the small blood volume. In a few patients, we tested 40-ml samples of blood with in vitro PAFC for 10 min per sample, giving us a sensitivity threshold estimated as 25 CTCs/liter. The correction of energy, putting chicken skin on the tube to model in vivo conditions, allowed us to estimate the false-negative rate of PAFC in vivo as 38% (±18% SE) due to the presence of low pigmented CTCs producing PA signals below the blood background.

Testing blood samples using other ex vivo CTC assays

Using fluorescence imaging (Fig. 4), CTCs were identified as nucleated cells [4′,6-diamidino-2-phenylindole–positive ($DAPI^+$)] having a relatively large size (12 to 20 μm)

compared to smaller (6 to 8 μm) RBCs and WBCs and lacking WBC receptors ($CD45^{-}$, red color), but expressing melanoma receptors ($MCSP^{+}$ and/or $CD146^{+}$, green color). In particular, cells with green emission (Fig. 4, A and B) were identified as CTCs, whereas cells with red emission were considered as WBCs expressing only CD45 (Fig. 4C). Cell fragments demonstrated no blue color (Fig. 4D) indicative of intact nuclei. We observed low and high intensity of green colors in many CTCs with high and low melanin content, respectively (Fig. 4, A and B, second column). This discovery of inverse correlation of melanin concentration and melanoma marker expression is in line with our preclinical studies, suggesting that (i) melanin synthesis is accompanied by suppression of melanoma marker expression and/or (ii) melanin can quench fluorescence, resulting in a dark ring around melanin granules (fig. S9). We also found CTC clusters ranging in sizes from 2 to 8 to 10 CTCs (Fig. 4, E to G). The viability test of isolated cells revealed that 89 ± 6.9% of WBCs and 56 ± 6.6% of CTCs were viable, suggesting that, although the preparation procedure can partly reduce the cell viability, the proportion of viable CTCs in circulation is lower than that of WBCs. In general, fluorescence imaging confirmed the presence of CTCs in several samples (for subjects 1, 2, 3, 4, and 7) when in vivo PAFC revealed high concentration of CTCs (>1 CTC/ml), which is also in line with data obtained with in vitro PAFC (table S2).

To estimate the accuracy of conventional flow cytometry, a controlled number of human CTCs were spiked into fresh blood from healthy individuals. These samples were processed to separate mononucleate cells such as WBCs from RBCs. Then, the samples were labeled by dyes allophycocyanin (APC) and PerCP-Cy5.5 conjugated with antibodies to target MCSP and CD146 melanoma cell markers, respectively. The WBCs were distinguished from CTCs by labeling them with anti-CD45 antibody and by immunohistochemical staining (Fig. 4H). To estimate the extent of false signals, cell suspensions (1 ml) in phosphate-buffered saline (PBS) and fresh blood (after separation of mononuclear cells) were initially tested by flow cytometry without any labeling. We used the channels that were applied for the detection of CTCs labeled by APC and PerCP-Cy5.5. For both samples, we obtained no false-positive signals for the APC channel and 0.1 to 0.3% of false-positive signals for the PerCp-Cy5.5 channel. The samples exhibiting higher numbers of events than this percentage were considered as CTC positive. Eventually, we estimated that using two melanoma markers allowed us to detect up to 78 ± 4% of melanoma CTCs in the samples from several patients with relatively high CTC content only (fig. S10 and table S4).

We also applied a MACS enrichment and detection kit using conjugated magnetic beads to target CTCs in blood from patients with melanoma (fig. S11 to S13). These data also confirmed the presence of CTCs in patients with a relatively high concentration of CTCs (>1 CTC/ml). Using spiked samples, the recovery rate was consistently more than 36% of tumor cells seeded in the blood samples with a mean of 40%. We additionally applied a conventional immunocytochemical staining procedure using the HiDef Detection HRP Polymer System and melanoma antibody cocktail containing HMB-45, MART-1, and tyrosinase to identify melanoma cells after magnetic separation. Our results revealed that this method allowed positive staining of 92% of the melanoma cells. In addition, we applied PT microscopy (7) to confirm the presence of pigmented CTCs or CTCs labeled with magnetic beads (fig. S11).

qRT-PCR was performed to test the expression of seven of the melanoma markers in 14 patients with melanoma after careful preclinical calibration. First, to evaluate sensitivity of the qRT-PCR method, blood samples from healthy volunteers (negative controls) were spiked with 100, 1000, or 10,000 cells from a human melanoma cell line. The obtained data indicate a positive relationship between the increasing number of spiked cells and higher expression of melanoma markers (fig. S14). *TGBF2* gene exhibited slightly different behavior. The results for expression of the above melanoma markers in the 14 patients are summarized in table S5.

In general, conventional assays failed to provide reliable data on the rare CTC presence due to their low sensitivity (table S6). Therefore, after first testing the stage III to IV patients with confirmed relatively high CTC concentrations, we stopped using most assays due to their low sensitivity and continued to use only in vitro PAFC.

Theranostic approach to CTCs

Over 1 hour of in vivo regular monitoring of the hand vessels, we observed that 6 among 18 patients showed some decreases in both the PA peak amplitudes and rates (fig. S6B). This finding suggests that CTCs have the potential to be theranostic targets, integrating PA detection and PT-based physical destruction of CTCs through nanobubble-induced photomechanical effects on CTC membranes and vital intra-cellular structures (7). Exposing the cubital vein [diameter, 3 to 4 mm; flow velocity, 7 to 8 cm/s (flow rate ~1.3 ml/s); blood volume assessed, 5 liters in 40 min] to a laser (Fig. 5, A and B) for 1 hour with the institutional review board (IRB)–approved laser energy notably decreased the CTC counts, up to a 48-fold reduction in one patient (Fig. 5, C and D). This result is likely related to the high melanin content in CTCs in that particular patient.

Then, we performed a similar procedure in vitro with PAFC (Fig. 3A) by monitoring CTC counts with low laser energy for 10 min (diagnostic mode), then with enhanced laser energy as in vivo for 1 hour (therapeutic mode), and then in diagnostic mode again. We estimated the ratio of CTC counts before and after the therapeutic procedure, revealing marked reductions of CTC counts in several samples, ranging from 2.8- to 11-fold (Fig. 5E), likely depending on the CTC melanin content and confirming the theranostic potential of the Cytophone platform. In addition, the monitoring of a blood sample in vitro with gradual increase in the energy fluence from 200 to 500 mJ/cm^2 demonstrated a nonlinear dependence of the number of PA peaks (CTCs) on the laser energy. We observed two different peak behaviors: (i) a nonlinear continuous increase with laser fluence (fig. S8C) that is in line with our previous finding (25, 29) and (ii) an initial increase followed by decrease as the laser fluence increases (fig. S8D). The latter behavior is associated with more effective photomechanical destruction of CTCs at higher laser energy for CTCs with high melanin content. The measurements of CTCs over a long time period (Fig. 5F) also demonstrated the ability of PAFC to monitor disease stage and potential need for additional treatment.

DISCUSSION

This work demonstrates a noninvasive in vivo blood test using our PAFC-based Cytophone diagnostic platform in clinical conditions to detect CTCs directly in the patient's bloodstream. It has the capability to improve the detection limit by ~1000 times compared to existing methods. This was performed through noninvasive, label-free detection of CTCs in 1.3- to 2.8-mm-diameter hand veins at a depth of 1 to 2 mm in patients with melanoma. The PAFC detection limit achieved in vivo is about 1 CTC/1000 ml or 130- to 1000-fold better than the sensitivity of CellSearch (1 CTC/7.5 ml) and other CTC assays (1 to 5 CTCs/ml) (1-4). As a result, we unambiguously observed CTCs in 96% of melanoma patients mostly with stage III and IV disease, whereas preexisting methods revealed the presence of CTCs in less than 40 to 60% of patients with cancer (15, 30, 31). Besides low sensitivity, inconsistent results among the various existing CTC assays create doubts regarding their clinical value (1, 5). The PAFC assay parameters that we optimized in the training set were tested on a validation set: an independent cohort of 10 patients. The data obtained from validation set confirmed the clinical potential of PAFC, with its high sensitivity and paucity of artifacts, which were easy to identify. We also observed white, likely platelet-rich CBCs in 22.2% of the first 18 patients, supporting previous discussions of the major role of thromboembolic complications in patients with cancer (20-22). Moreover, even healthy participants had small but detectable CBCs, which could be associated with normal physiological process or response to minor unidentified internal pathological events. If CBCs are small enough, then they can be broken down via fibrinolysis. However, in many cases, small CBCs could precede formation of large CBCs or aggregation of small CBCs (20-23). Thus, high-sensitivity PAFC, which can detect small CBCs, has a potential to help medical researchers establish lower and upper limits of normal CBC counts in healthy participants, which could then be used as benchmarks for evaluating a patient's health and risks. Thus, monitoring the size and number of CBCs may reduce the risk of pulmonary embolism, stroke, or other thromboembolic diseases by well-timed anticoagulant therapy and potentially optimize this therapy through real-time CBC counting, which is impossible with existing approaches. Taking into account PAFC's resolution, we can estimate the minimal detectable size of a CBC as 30 μm (±SE of 6 μm).

Our preclinical study (7, 8) revealed the potential of PAFC for real-time monitoring of CTCs released from a small (0.4 to 1 mm) metastatic tumor that can produce many (hundreds and more) CTCs every day. Thus, CTCs can be detected with PAFC in individuals before their primary tumor is diagnosed with existing techniques or causes apparent symptoms. Moreover, our preclinical studies (7, 8, 29) and data presented here revealed the potential of photomechanical destruction of melanoma CTCs through laser-induced nanobubbles around overheated melanin clusters that can reduce CTC count by an average of 10- to 15-fold and more for highly pigmented CTCs. These CTC reductions were seen at a relatively low laser energy approved for the PAFC diagnostic mode. The laser energy was not yet optimized for therapeutic application in humans, and this will need to be done in the future.

This theranostic platform can potentially reduce the risk of metastasis and rapidly treat surgery-induced CTCs (32, 33). The CTC clusters and CTC-CBC emboli had slower velocities than single CTCs measured with PA time-of-flight techniques (7), likely due to

their larger size or the effects of rolling along the blood vessel wall, which can enhance CTC extravasation and, hence, metastasis formation.

Thus, PAFC can be applied for early melanoma diagnosis, follow-up monitoring of melanoma recurrence, and selection of more effective therapy through monitoring of CTC counts and PAFC-guided CTC theranostics. Melanoma is a good target for exploring the clinical potential of a PAFC blood test because it can provide label-free diagnosis of a ≤1-mm tumor frequently undetectable with existing methods. Using PAFC technology, the role of CTCs for early diagnosis and metastasis prevention can be carefully estimated and compared to the use of circulating DNA and/or exosomes as cancer markers. Note that DNA likely cannot be considered as a metastatic marker because only viable CTCs can create metastasis. In addition, according to our preclinical data (34), exosomes are released from a primary tumor at a similar or earlier time and in higher concentration than CTCs, but the identification of tumor-derived exosomes and DNA is extremely difficult against a large background from normal cells (1, 34).

PAFC in a label-free mode can be applied only to targets with natural PA contrasts such as melanoma cells with intrinsic melanin content. In vivo PAFC's false-negative rate ± SE is 38 ± 18% CTCs, due to low melanin content creating signals below blood background, which is in line with our previous data on animal models (7, 8). Nevertheless, this can be considered as appropriate because existing CTC assays have much higher false negativity due to smaller blood volume (1 to 10 ml versus 300 to 1000 ml), low marker expression (for example, EpCAM), and CTC losses during sample processing (1). Although optical clearing provided a two- to threefold increase in PA signal amplitude in the training group, the high sensitivity of PAFC allowed us to exclude this relatively time-consuming procedure in the validation group. In label-free mode, without any artificial contrast agents, a PAFC-based blood test could be applicable to high-sensitivity detection of CBCs for potential stroke prevention (23), sickle cells (35), and malaria (24), where the expected 10,000-fold sensitivity improvement could provide both early diagnosis and a means to block malaria transmission. Beyond melanoma, PAFC can be extended to other cancers through molecular targeting of CTCs with functionalized gold nanoparticles as PA contrast agents (36) and spasers (37, 38), some of which are already approved for pilot clinical trials (39). Nevertheless, full approval to use nanoparticles in humans will require additional time. Further studies should show whether PAFC-based early diagnosis integrated with the killing of CTCs by laser could be effective for cancer treatment alone or in combination with conventional therapies and whether some reduction in CTC numbers could at least inhibit the progression of metastasis.

MATERIALS AND METHODS

Study design

A total of 47 participants including 19 healthy individuals (14 Caucasian and 5 African-American) and 28 patients with melanoma mostly at stages III and IV with light skin (Fitzpatrick scale type I or II) were recruited. This was a nonrandomized, nonblinded study using the PAFC setup (figs. S1 and S2) according to a protocol that was approved by the IRB at the University of Arkansas for Medical Sciences (UAMS). The healthy

individuals and patients were seated in a chair. For participants with a tremor, the examined hand was gently fixed with a customized holder (fig. S1C, Jaeco Orthopedic Inc.). The position of the holder and hand was adjusted using a customized XYZ translation stage (XYZ-4400ML, Conix Research Inc.) controlled by a joystick. The transducer was mounted on an independent small XYZ stage to allow micrometer-precision adjustment of its spatial position. The PA probe was positioned on the participant's skin above the selected vein (Fig. 1A and fig. S1B). Standard ultrasound gel provided acoustic coupling between the transducer and the skin. Spatial navigation of the PA probe on the vein was controlled by conventional ultrasound imaging and by time-resolved detection of PA signals from skin and vein coming to the transducer with a time delay. Optical clearing was applied to the skin to improve light penetration into tissue by minimizing light scattering.

In vivo PAFC clinical setup

The PAFC clinical prototype (Fig. 1 and figs. S1 and S2) was built using a near-infrared ytterbium-fiber laser (model YLPM-0.3-A1-60-18, IPG Photonics Corp.) with the following parameters: wavelength, 1060 nm; pulse width, 0.8, 5, and 10 ns; pulse repetition rate, 10 to 600 kHz; and pulse energy, up to 300 μJ. To minimize the overheating of superficial skin, the pulse repetition rate was adjusted to 1 kHz by incorporation of a mechanical chopper (MC2000B, Thorlabs Inc.). A collinear continuous wave pilot laser with wavelength of 635 nm and power of 2 mW (model CPS180, Thorlabs Inc.) after 757-nm dichroic mirror (Semrock Inc.) was adjusted collinearly with a near-infrared laser beam for navigation and visualization of laser beam positions on the samples. An assembly of aspheric (C560TME-C) and cylindrical (LJ1310-L1-C) lenses (Thorlabs Inc.) formed a linear laser beam with dimensions of 16 μm by 880 μm.

Laser-induced acoustic waves, referred to as PA signals, were detected by the customized focused cylindrical transducers using a 28-μm-thick polyvinylidene fluoride film with a broadband frequency response in the range of 0.2 to 32 MHz and a focal length of 6 mm with and without a central hole to deliver a laser beam to skin. This schematic called acoustic resolution PAFC (7) provided a high acoustic resolution at a level of 65 μm at a tissue depth of 1 to 3 mm. A standard ultrasound gel (Aquasonic Clear, Parker Labs Inc.) was used for acoustic coupling between the transducer and the skin. The position of the laser beam and transducer was adjusted using an XYZ translation stage (Conix Research Inc.) controlled by a joystick or computer. The transducer signals were preamplified using a 20-dB amplifier (model AH-2010-100, Onda Corp.). A standard ultrasound medical imaging system (M7, Mindray DS Inc.) was used for visualization of the selected veins, their size, depth, and flow velocity and preliminary guidance of PAFC system.

The PAFC acquisition system consisted of a data acquisition board (ATS9350, Alazar Technologies Inc.), a workstation (Precision T3500, Dell Technologies Inc.), a pulse generator (DG645, Stanford Research Systems Inc.), and a photodetector (PDA10A, Thorlabs Inc.). The software was developed in MATLAB (MathWorks Inc.). The laser was triggered at a fixed rate of 10 kHz. A chopper was used to lower the laser pulse rate at the sample, if needed. The photodetector placed after the chopper triggered the data acquisition. PA signals were sampled at a rate of 500 MHz. A number of consecutive PA

signals (typically, 4 to 20) were averaged to increase the signal-to-noise ratio and recorded before further processing. Next, the PA signal waveforms (Fig. 2, B and C, and fig. S4A) were transformed to PA traces, in which each PA signal waveform was represented as a single point in a PA trace. The trace's baseline corresponded to background signals from the blood vessel. Any targets in the flow such as CTCs, which produced a stronger signal than blood, appeared as transient peaks in the trace. The width of these peaks corresponded to the time of flight of the CTCs through the detection volume. Thus, the original PA signals with classical positive and negative components (fig. S4A) were transformed into transient PA peaks in the signal trace (Fig. 1D) as in conventional flow cytometry.

In the next step, the trace was filtered using a high-pass filter (10 Hz cutoff frequency) to eliminate background fluctuations before peak detection. The threshold for peak detection was determined by $PA_{th} = m + k*IQR$, where m is the median and IQR is the interquartile range of the trace. k is a constant determined from control experiments. Depending on the blood vessel's size and other features (movements, flow dynamics, etc.) of in vivo measurements, the envelope of background signals in the PA trace may vary widely. To overcome this variation, the PA trace was analyzed in 10-s-long windows, and threshold was recalculated in each window. Once the peaks were identified, their properties (normalized amplitude, full width at half maximum) were also measured.

Last, we manually checked for artifacts after the automatic detection (postprocessing procedure). PA signals that were behind each detected peak were visualized. If the signal was deemed to be an artifact, then the associated peak was excluded from the results.

In vitro PAFC device

Blood samples from patients were tested in vitro using two different PAFC setups. The first setup (Fig. 3, A and B) was identical to the in vivo PAFC setup and used a glass tube with inner diameter of 0.8 mm and length of 10 cm (Corning Inc.) as the vessel phantom. Blood samples (EDTA tube) in volumes of 1 to 6 ml and up to 40 ml in two experiments were each pumped through the tube by a variable-flow peristaltic pump (model 13-876-1, Thermo Fisher Scientific Inc.) at a linear flow velocity of 10 mm/s (rate of ~0.3 ml/min). Deionized water was used for acoustic coupling between the focused ultrasound transducer and the tube phantom. The glass tube, transducer, and optical focusing system were immersed into the water. The PA signals were detected with a cylindrical ultrasound transducer (32 MHz; focal length, 8 mm) located in a water bolus around the tube. The PA signal rate (CTCs/ml) as a function of laser energy fluence was studied for pulse-energy fluences of 200, 300, 400, and 500 mJ/cm^2.

In the second in vitro PAFC setup (fig. S7, A to D), the laser (MOPA-M-10, Multiwave Photonics S.A.) had the following properties: wavelength, 1064 nm; pulse width, 10 ns; pulse rate, 2 kHz; and a maximal pulse energy of 350 μJ, which was adjusted using natural density filters. The laser beam was focused into a line with dimensions of 12 μm by 210 μm. Acoustic waves were detected with an ultrasound transducer [lateral resolution, 120 μm; focal length, 12 mm; frequency band, 10 MHz (V316, Olympus NDT Inc.)] and then acquired by a digitizer (PCI-5152, National Instruments Corp.). Signal acquisition and analysis were performed using software (LabVIEW, National Instruments Corp.).

Cells

HTB-65 and A2058 human melanoma cell lines and B16F10 mouse melanoma cell line (both from American Type Culture Collection) were cultured using standard procedures per the vendor's specifications.

Optical skin clearing

This procedure was described elsewhere (28). It includes the cleaning, microabrasion, application of clearing agents, and the diffusion enhancement procedure. Briefly, the skin was first wiped using medical 95% ethyl alcohol (190 proof) applied topically for 2 min. Second, a thin skin layer (stratum corneum) was removed with a professional grade Diamond Microdermabrasion Machine for 2 min (NV-07D, HealthAndMed Corp.). Third, 99% glycerol (Sigma-Aldrich Inc.) was topically applied to the skin followed by sonophoresis (Sonicator 740, Mettler Electronics Corp.) for 6 min.

Blood sample collection and processing

A total of 10 to 40 ml of blood was collected from each participant in EDTA tubes (BD Biosciences Inc.). Samples were examined ex vivo using six in vitro CTC assays to verify in vivo data.

Patient medication

During the study, one participant took aspirin (Aspirin Regimen Bayer Low Dose Safety Coated Aspirin, 81 mg tablets; Bayer Healthcare Pharmaceuticals Inc.) at one tablet/day for a 6-week period.

Magnetic-activated cell sorting

Magnetic MACS MS Columns (Miltenyi Biotec Inc.) were used for cell separation. To extract mononucleated blood components, 1 ml of whole blood and 1 ml of PBS were combined and gently layered on top of 1.5 ml of Ficoll-Paque Premium (catalog no. 07908, StemCell Technologies). Samples were centrifuged at 400*g* for 30 min at room temperature. The upper plasma layer was carefully removed and discarded, and the middle (mononucleated) region was extracted and placed in a new centrifuge tube. Mononucleated samples were washed once with running buffer (catalog no. 130-091-221, Miltenyi Biotec Inc.) that had been degassed by filtering the buffer through a 0.22-μm bottle-top filter. Cells were concentrated to a final volume of 300 μl. For magnetic labeling of melanoma CTCs, the WBC-CTC fraction was resuspended in 300 μl of PBS, mixed with Anti-Melanoma (MCSP) MicroBeads, and incubated for 30 min at 4°C. Cells were washed once and then resuspended in 500 μl of PBS supplemented with 2 mM EDTA. For magnetic separation of melanoma cells, the cell suspension was passed over a MS+ separation column (Miltenyi Biotec Inc.) placed in the magnetic field of an OctoMACS separator (Miltenyi Biotec Inc.). Labeled cells were attached to the magnetized matrix in the column, whereas unlabeled cells were removed by washing out with PBS supplemented with 2 mM EDTA and 0,5% bovine serum albumin (BSA) and then collected as the negative fraction. The separation column was removed from the magnet, and the retained cells were flushed from the column with 500 μl of PBS supplemented with 2 mM EDTA and 0.5% BSA and collected as the positive

fraction. Cells isolated by MACS were attached to microscopic glass using Cytospin and then air-dried for 1 hour at room temperature. In recovery experiments, different numbers of HTB-65 cells (100, 10, and 1) were added to 1 ml of blood from healthy volunteers. Another blood sample with no added tumor cells served as a control. The experiments were done under identical conditions as described above and repeated five times.

Immunocytochemical staining

Cells isolated from MACS were fixed with a fixation reagent and blocked with a peroxidase blocker (both from Enzo Life Sciences Inc.). Samples were stained using melanoma cocktail: primary antibodies (to HMB-45, MART-1, and tyrosinase), HiDef Detection HRP Polymer System, and a DAB kit (Cell Marque Corporation). Cells were counterstained with hematoxylin and eosin stain. Brown staining of cells was assessed by light microscopy.

In a separate experiment, the samples were stained with CD45-VioBlue and MCSP-APC to detect the presence of leukocytes and melanoma cells, respectively. Samples were visualized using transmission and fluorescent microscopy with various exposure times.

qRT-PCR analysis

Blood from participants was collected in PAXgene Blood RNA tubes, and total RNA was isolated using the PAXgene Blood RNA Kit (Qiagen Inc.); RNase-free deoxyribonuclease was used to ensure removal of any traces of genomic DNA contamination. RNA was quantified, and the quality of RNA was checked with an Agilent 2100 Bioanalyzer (Agilent Technologies Inc.); all samples exhibited high quality (RNA integrity number, >8). For the following qRT-PCR procedures, all supplies were purchased from Invitrogen. First-strand complementary DNA (cDNA) was synthesized using 1 μg of total RNA and random primers with either Superscript VILO (for direct qPCR) or High Capacity cDNA Synthesis kit (for qPCR after performing a preamplification step). For the preamplification step, 250 ng of cDNA was amplified using TaqMan PreAmp Master Mix and a pool of the seven melanoma markers *ABCB5*, *MAGEA3*, *MCAM*, *MLANA2*, *PAX3*, *TGFB2*, and *TYR2* and the housekeeping gene *GAPDH*. The qRT-PCR was then performed using 100 ng of either regular cDNA or preamplified cDNA as the template with TaqMan Gene Expression Master Mix. The qRT-PCR was performed on ABI 7900HT (Applied Biosystems Inc.), with all data determined in exponential phase of the reactions. Data were analyzed using the comparative Ct method. The C_t values of housekeeping gene *GAPDH* was first subtracted from the C_t values for each of the melanoma marker target genes (ΔC_t), and then, the ΔC_t values of the healthy negative-control subjects (as calibrator) was subtracted from the ΔC_t values for the patients resulting in $\Delta\Delta C_t$ values. Fold changes were then calculated as 2 to the power of negative $\Delta\Delta C_t$.

Flow cytometry in vitro

Flow cytometry analysis was performed using BD LSRFortessa X-20 flow cytometer (BD Biosciences Inc.). For this purpose, 1 ml of blood from patients with melanoma was used. Sizes of 8 to 25 μm were associated with individual mononuclear ceEs such as WBCs and melanoma CTCs. Additional healthy blood samples (1 ml) served as a positive control for spiking and recovery experiments using the human melanoma cell line (HTB-65 from

American Type Culture Collection). In spiking experiments, the melanoma cells from the human melanoma cell line were cultured according to the vendor's specifications. Viable cells were resuspended in PBS. To determine the sensitivity and specificity of flow cytometry, the following samples were prepared: (i) 1×10^5 melanoma cells in 1 ml of PBS; (ii) 1×10^5 melanoma cells in 1 ml of PBS labeled with 1 μg of antibody to CD45, MCSP, and CD146; (iii) 1 ml of healthy blood labeled with 1 μg of CD45, MCSP, and CD146; (iv) 1×10^5 tumor cells spiked in 1 ml healthy blood without labeling; (v) controlled number of melanoma cells (1×10^5, 1×10^3, 1×10^2, and 1×10^1) spiked with 1 ml of healthy blood and labeled with antibody to CD45, MCSP, and CD146 each.

Fluorescence imaging

For fluorescence imaging, mononuclear cells isolated from 100 μl of whole blood from each patient were labeled, fixed, and analyzed on the slides. Imaging was performed using an Olympus IX81 inverted microscope equipped with a cooled color charge-coupled device camera (DP72, Olympus Corp.). Images were obtained in either transmission (bright field) mode or fluorescence mode with an emission filter of 530 ± 30 nm (for FITC label) and 575 ± 30 nm (for PE label). To identify nuclei, cells were additionally labeled with DAPI (Invitrogen Corp.). Images were acquired and combined (if necessary) at a workstation and processed in Adobe Photoshop (Adobe Inc.) and ImageJ 1.46 for Windows (available at http://rsb.info.nih.gov/ij/). Melanoma CTCs were distinguished as $MCSP^+/CD146^+/CD45^-DAPI^+$, $MCSP^+/CD146^-/CD45^-/DAPI^+$, or $MCSP^-/CD146^+/CD45^-/DAPI^+$ as compared to $CD45^+$ normal WBCs and $DAPI^-$ fragments of cells.

Statistics

MATLAB 8.3 (MathWorks Inc.), Excel 2013 (Microsoft Corp.), and SAS Enterprise Guide 7.1 (SAS Institute Inc.) were used for statistical analyses. Most patients with melanoma and healthy volunteers had blood volumes available for testing in vitro. In patients with melanoma, the numbers of CTCs detected were assumed to follow Poisson distributions with intensity parameters that varied among patients. Accordingly, the CTC concentration, λ_i, and ±SE of λ_i [±SE(λ_i)] in the ith patient was estimated as $\lambda_i \pm \mathrm{SE}(\lambda_i) = (N_i \pm \sqrt{N_i}) / V_i$, where N_i and V_i are the number of CTC-associated PA peaks detected and the volume (in milliliters) of blood that was monitored in the ith patient, respectively. Among healthy volunteers, the number of false-positive CTCs detected was assumed to follow a single Poisson distribution whose intensity parameter, being reflective of the detection system, was constant across volunteers. Accordingly, the estimate ± SE of the false-positive rate, $\lambda_S \pm \mathrm{SE}(\lambda_S)$, was calculated as $\lambda_S \pm \mathrm{SE}(\lambda_S) = (N_S \pm \sqrt{N_S}) / V_S$, where N_S and V_S are the total number of false-positive PA peaks detected and the total volume (in milliliters) of blood that was monitored in the set of healthy volunteers, respectively. Patient detection rates λ_i and the false-positive rate λ_S were used to score patients for whether CTCs were detected ("Patient Result") as follows: if the difference $\delta_i = \lambda_i - \lambda_S$ was >2 times the SE(δ_i) of this difference, then the Patient Result was Yes, CTCs were detected. SE (δ_i) was calculated as $\mathrm{SE}(\delta_i) = \sqrt{\mathrm{SE}^2(\lambda_i) + \mathrm{SE}^2(\lambda_S)}$, where $\mathrm{SE}^2(°)$ represents a squared SE. The correlation between λ_i measured using in vivo PAFC versus in vitro PAFC was assessed with Spearman correlation. Agreement in patient results determined from in vivo PAFC

versus in vitro PAFC was assessed using the number (percent) of concordant results along with Cohen's κ.

Supplementary Material

Refer to Web version on PubMed Central for supplementary material.

Acknowledgments:

We thank K. Simpson, K. Morehead, K. Mack, A. Annis, T. Mack, N. Harris, and A. Trammel from the UAMS clinical team for the support of this study. We also thank the UAMS laser safety committee and especially S. Fergusson for the support in laser safety control, I. Pelivanov for providing the customized focused cylindrical transducers, and Jaeco Orthopedic Inc. for designing the hand holder.

Funding:

This work was supported, in part, by the RF grant 14.Z50.31.0044, the NIH grants R01CA131164 and R01EB017217, and by the NSF grants OIA 1457888 and DBI 1556068.

REFERENCES AND NOTES

1. Alix-Panabières C, Pantel K, Challenges in circulating tumour cell research. Nat. Rev. Cancer 14, 623–631 (2014). [PubMed: 25154812]
2. Ashworth TR, A case of cancer in which cells similar to those in the tumors were seen in the blood after death. Aust. Med 114, 146–149 (1869).
3. Cristofanilli M, Budd GT, Ellis MJ, Stopeck A, Matera J, Miller MC, Reuben JM, Doyle GV, Allard WJ, Terstappen LWMM, Hayes DF, Circulating tumor cells, disease progression, and survival in metastatic breast cancer. N. Engl. J Med 351, 781–791 (2004). [PubMed: 15317891]
4. Hong B, Zu Y, Detecting circulating tumor cells: Current challenges and new trends. Theranostics 3, 377–394 (2013). [PubMed: 23781285]
5. Gorges TM, Penkalla N, Schalk T, Joosse SA, Riethdorf S, Tucholski J, Lücke K, Wikman H, Jackson S, Brychta N, von, Ahsen O, Schumann C, Krahn T, Pantel K, Enumeration and molecular characterization of tumor cells in lung cancer patients using a novel in vivo device for capturing circulating tumor cells. Clin. Cancer Res 22, 2197–2206 (2016). [PubMed: 26667488]
6. Chen S, El-Heliebi A, Tauber G, Langsenlehner T, Pötscher M, Kashofer K, Czyż ZT, Polzer B, Riethdorf S, Kuske A, Leitinger G, Pantel K, Kroneis T, Sedlmayr P, Catch and release: Rare cell analysis from a functionalised medical wire. Sci. Rep 7, 43424 (2017). [PubMed: 28233867]
7. Galanzha EI, Zharov VP, Circulating tumor cell detection and capture by photoacoustic flow cytometry in vivo and ex vivo. Cancer 5, 1691–1738 (2013).
8. Galanzha EI, Shashkov EV, Spring PM, Suen JY, Zharov VP, In vivo, noninvasive, label-free detection and eradication of circulating metastatic melanoma cells using two-color photoacoustic flow cytometry with a diode laser. Cancer Res. 69, 7926–7934 (2009). [PubMed: 19826056]
9. Bell AG, On the production and reproduction of sound by light. Am. J. Sci 20, 305–324 (1880).
10. Zharov VP, Letokhov VS, Laser Optoacoustic Spectroscopy (Springer, 1984) vol. 37.
11. Knieling F, Neufert C, Hartmann A, Claussen J, Urich A, Egger C, Vetter M, Fischer S, Pfeifer L, Hagel A, Kielisch C, Görtz RS, Wildner D, Engel M, Röther J, Uter W, Siebler J, Atreya R, Rascher W, Strobel D, Neurath MF, Waldner MJ, Multispectral optoacoustic tomography for assessment of Crohn's disease activity. N. Engl. J. Med 376, 1292–1294 (2017). [PubMed: 28355498]
12. Ermilov SA, Khamapirad T, Conjusteau A, Leonard MH, Lacewell R, Mehta K, Miller T, Oraevsky AA, Laser optoacoustic imaging system for detection of breast cancer. J. Biomed. Opt 14, 024007 (2009). [PubMed: 19405737]
13. Stoffels I, Morscher S, Helfrich I, Hillen U, Leyh J, Burton NC, Sardella TCP, Claussen J, Poeppel TD, Bachmann HS, Roesch A, Griewank K, Schadendorf D, Gunzer M, Klode J, Metastatic status

of sentinel lymph nodes in melanoma determined noninvasively with multispectral optoacoustic imaging. Sci. Transl. Med 7, 317ra199 (2015).

14. Petrov YY, Petrova IA, Patrikeev IA, Esenaliev RO, Prough DS, Multiwavelength optoacoustic system for noninvasive monitoring of cerebral venous oxygenation: A pilot clinical test in the internal jugular vein. Opt. Lett 31, 1827–1829 (2006). [PubMed: 16729084]
15. Mocellin S, Hoon D, Ambrosi A, Nitti D, Rossi CR, The prognostic value of circulating tumor cells in patients with melanoma: A systematic review and meta-analysis. Clin. Cancer Res 12, 4605–4613 (2006). [PubMed: 16899608]
16. Flaherty KT, Infante JR, Daud A, Gonzalez R, Kefford RF, Sosman J, Hamid O, Schuchter L, Cebon J, Ibrahim N, Kudchadkar R, Burris HA III, Falchook G, Algazi A, Lewis K, Long GV, Puzanov I, Lebowitz P, Singh A, Little S, Sun P, Allred A, Ouellet D, Kim KB, Patel K, Weber J, Combined BRAF and MEK inhibition in melanoma with BRAF V600 mutations. N. Engl. J. Med 367, 1694–1703 (2012). [PubMed: 23020132]
17. Weintraub K, Drug development Releasing the brakes. Nature 504, S6–S8 (2013). [PubMed: 24352363]
18. Wolchok JD, Kluger H, Callahan MK, Postow MA, Rizvi NA, Lesokhin AM, Segal NH, Ariyan CE, Gordon R-A, Reed K, Burke AM, Caldwell A, Kronenberg SA, Agunwamba BU, Zhang X, Lowy I, Inzunza HD, Feely W, Horak CE, Hong Q, Korman AJ, Wigginton JM, Gupta A, Sznol M, Nivolumab plus ipilimumab in advanced melanoma. N. Engl. J. Med 369, 122–133 (2013). [PubMed: 23724867]
19. Lu H, Liu S, Zhang G, Wu B, Zhu Y, Frederick DT, Hu Y, Zhong W, Randell S, Sadek N, Zhang W, Chen G, Cheng C, Zeng J, Wu LW, Zhang J, Liu X, Xu W, Krepler C, Sproesser K, Xiao M, Miao B, Liu J, Song CD, Liu JY, Karakousis GC, Schuchter LM, Lu Y, Mills G, Cong Y, Chernoff J, Guo J, Boland GM, Sullivan RJ, Wei Z, Field J, Amaravadi RK, Flaherty KT, Herlyn M, Xu X, Guo W, PAK signalling drives acquired drug resistance to MAPK inhibitors in SRAf-mutant melanomas. Nature 550, 133–136 (2017). [PubMed: 28953887]
20. A. Khorana A, Francis CW, Culakova E, Kuderer NM, Lyman GH, Thromboembolism is a leading cause of death in cancer patients receiving outpatient chemotherapy. J. Thromb. Haemost 5, 632–634 (2007). [PubMed: 17319909]
21. Sparsa A, Durox H, Doffoel-Hantz V, Munyangango E-M, Bédane C, Cendras J, Gantois C, Boulinguez S, Bonnetblanc J-M, High prevalence and risk factors of thromboembolism in stage IV melanoma. J. Eur. Acad. Dermatol. Venereol 25, 340–344 (2011). [PubMed: 20629849]
22. Uchino K, The balance of risk of bleeding and thrombosis in melanoma patients with brain metastases. Melanoma Res. 23, 82 (2013). [PubMed: 23196331]
23. Juratli MA, Menyaev YA, Sarimollaoglu M, Siegel ER, Nedosekin DA, Suen JY, Melerzanov AV, Juratli TA, Galanzha EI, Zharov VP, Real-time label-free embolus detection using in vivo photoacoustic flow cytometry. PLOS ONE 11, e0156269 (2016). [PubMed: 27227413]
24. Menyaev YA, Carey KA, Nedosekin NA, Sarimollaoglu M, Galanzha EI, Stumhofer JS, Zharov VP, Preclinical photoacoustic models: Application for ultrasensitive single cell malaria diagnosis in large vein and artery. Blomed. Opt. Express 7, 3643–3658 (2016).
25. Sarimollaoglu M, Nedosekin DA, Menyaev YA, Juratli MA, Zharov VP, Nonlinear photoacoustic signal amplification from single targets in absorption background. Photoacoustics 2, 1–11 (2014). [PubMed: 24921062]
26. Jawad HJ, Sarimollaoglu M, Biris AS, Zharov VP, Dynamic blood flow phantom with negative and positive photoacoustic contrasts. Blomed. Opt. Express 9, 4702–4713 (2018).
27. Bohndiek SE, Bodapati S, Van De Sompel D, Kothapalli S-R, Gambhir SS, Development and application of stable phantoms for the evaluation of photoacoustic imaging instruments. PLOS ONE 8, e75533 (2013). [PubMed: 24086557]
28. Menyaev YA, Nedosekin DA, Sarimollaoglu M, Juratii MA, Galanzha EI, Tuchin VV, Zharov VP, Optical clearing in photoacoustic flow cytometry. Blomed. Opt. Express 4, 3030–3041 (2013).
29. Kim J-W, Galanzha EI, Zaharoff DA, Griffin RJ, Zharov VP, Nanotheranostics of circulating tumor cells, infections and other pathological features in vivo. Mol. Pharm 10, 813–830 (2013). [PubMed: 23379366]

30. Kowalik A, Kowalewska M, Góźdź S, Current approaches for avoiding the limitations of circulating tumor cells detection methods—Implications for diagnosis and treatment of patients with solid tumors. Transl. Res 185, 58–84.e15 (2017). [PubMed: 28506696]

31. Khoja L, Lorigan P, Dive C, Keilholz U, Fusi A, Circulating tumour cells as tumour biomarkers in melanoma: Detection methods and clinical relevance. Ann. Oncol 26, 33–39 (2015). [PubMed: 24907634]

32. Martin OA, Anderson RL, Narayan K, MacManus MP, Does the mobilization of circulating tumour cells during cancer therapy cause metastasis? Nat. Rev. Clin. Oncol 14, 32–44 (2017). [PubMed: 27550857]

33. Juratli MA, Sarimollaoglu M, Siegel ER, Nedosekin DA, Galanzha EI, Suen JY, Zharov VP, Real-time monitoring of circulating tumor ceil release during tumor manipulation using in vivo photoacoustic and fluorescent flow cytometry. Head Neck 36, 1207–1215 (2014). [PubMed: 23913663]

34. Nolan J, Sarimollaoglu M, Nedosekin DA, Jamshidi-Parsian A, Galanzha EI, Kore RA, Griffin RJ, Zharov VP, In vivo flow cytometry of circulating tumor-associated exosomes. Anal. Cell. Pathol. (Amst.) 2016, 1628057 (2016). [PubMed: 27965916]

35. Cai C, Nedosekin DA, Menyaev YA, Sarimollaoglu M, Proskumin MA, Zharov VP, Photoacoustic flow cytometry for single sickle cell detection in vitro and in vivo. Anal. Cell. Pathol. (Amst.) 2016, 2642361 (2016). [PubMed: 27699143]

36. Galanzha EI, Shashkov EV, Kelly T, Kim J-W, Yang L, Zharov VP, In vivo magnetic enrichment and multiplex photoacoustic detection of circulating tumour cells. Nat. Nanotechnol 4, 855–860 (2009). [PubMed: 19915570]

37. Galanzha EI, Weingold R, Nedosekin DA, Sarimollaoglu M, Nolan J, Harrington W, Kuchyanov AS, Parkhomenko RG, Watanabe F, Nima Z, Biris AS, Plekhanov AI, Stockman MI, Zharov VP, Spaser as a biological probe. Nat. Commun 8, 15528 (2017). [PubMed: 28593987]

38. Alix-Panabières C, Pantel K, Here comes the spaser. Nat. Mater 16, 790–791 (2017). [PubMed: 28748959]

39. Shao J, Griffin RJ, Galanzha EI, Kim J-W, Koonce N, Webber J, Mustafa T, Biris AS, Nedosekin DA, Zharov VP, Photothermal nanodrugs: Potential of TNF-gold nanospheres for cancer theranostics. Sci. Rep 3, 1293 (2013). [PubMed: 23443065]

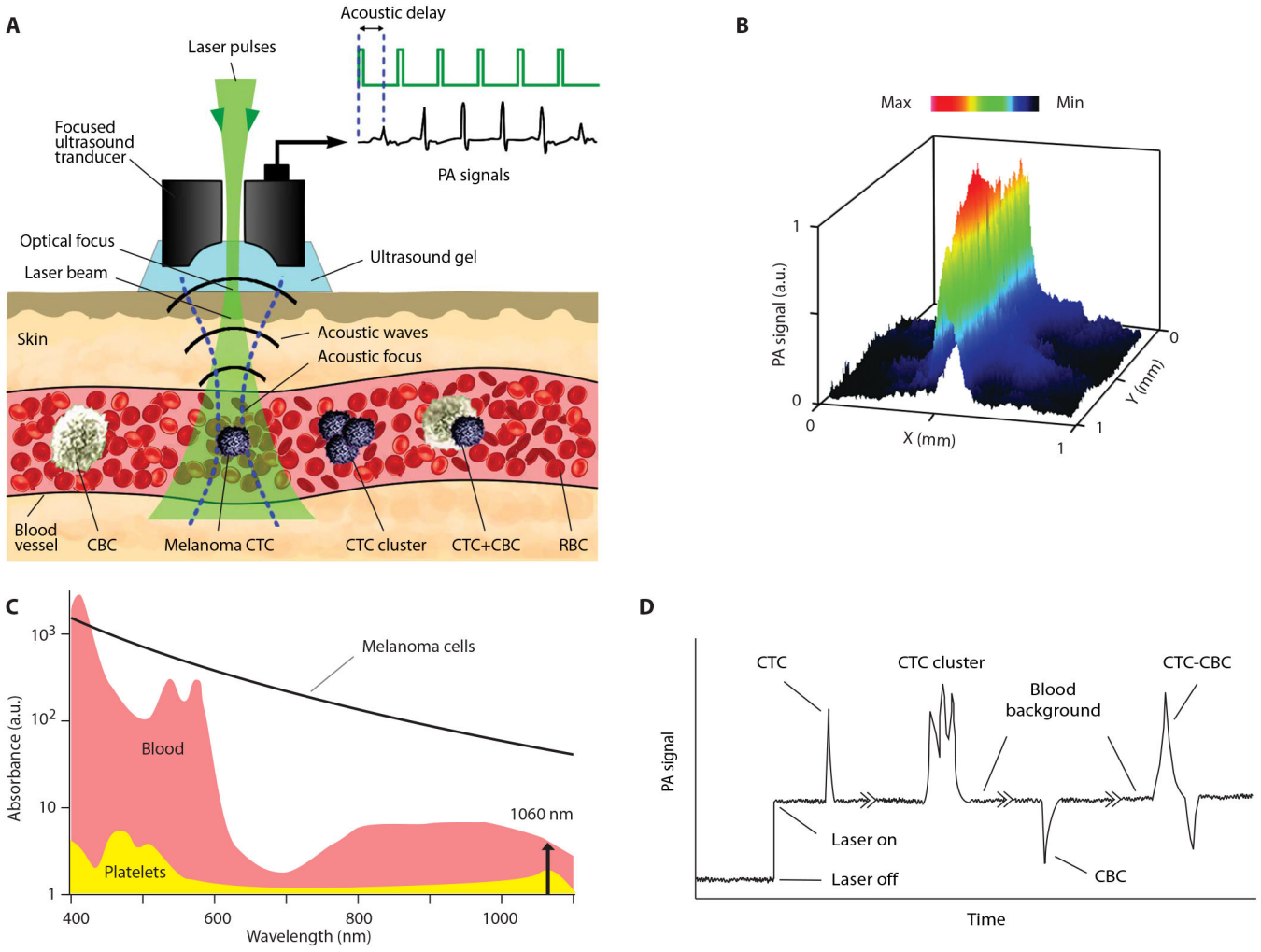

Fig. 1. The principle of CTC and CBC detection with the Cytophone platform using acoustic resolution PAFC.

(**A**) The schematic shows a focused ultrasound transducer with a central hole. Because of strong light scattering in tissue, the spatial resolution is determined by the acoustic focal volume. Laser-induced acoustic waves (referred to as PA signals) travel to the transducer with an acoustic time delay compared to laser pulse and PA background signals from the skin layer (23). (**B**) The lateral resolution (65 ± 6 μm) of the cylindrical transducer is shown as a PA signal distribution from black tape scanned with a focused laser beam with a diameter of 2 μm and a wavelength of 532 nm. a.u., arbitrary units. (**C**) The absorption spectra of RBCs (red), melanoma CTCs (black), and platelets (yellow) as the main components of white CBCs (7, 8, 23). (**D**) Left to right: PA trace with two positive PA peaks from a single CTC and a CTC cluster with three peaks above blood background and noise level, a negative PA peak from platelet-rich (white) CBC, and a peak with combined negative-positive contrast from CTC-CBC emboli (7, 23).

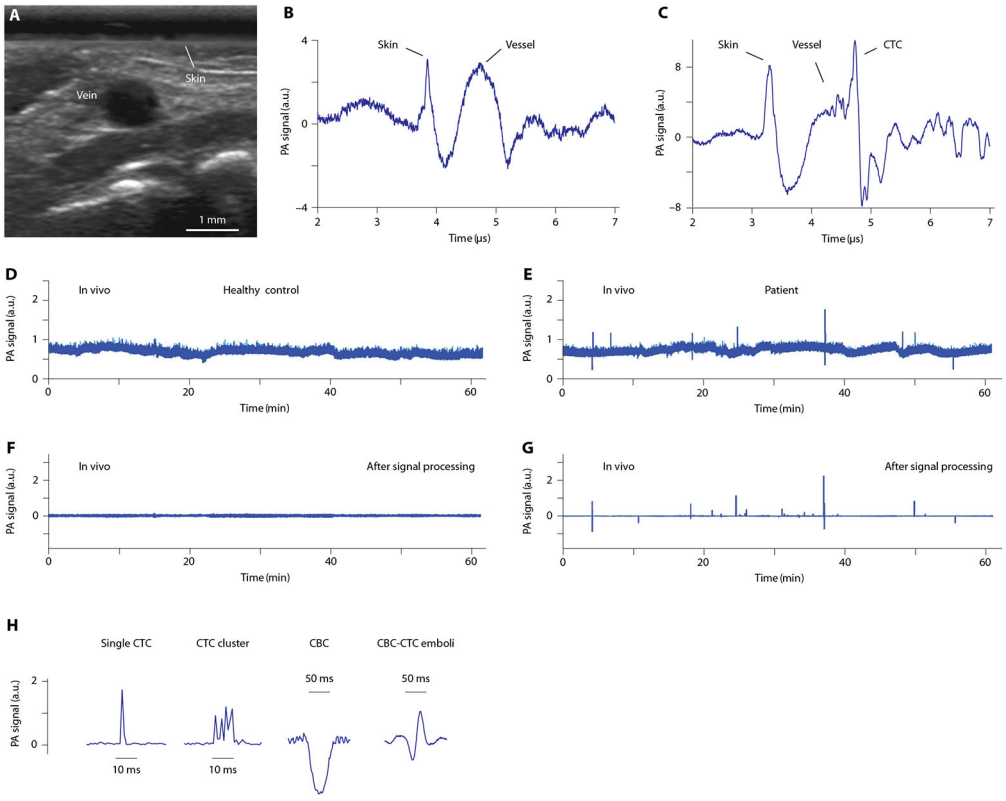

Fig. 2. In vivo PA detection of CTCs, CBCs, and CTC-CBC emboli in healthy volunteers and patients.

(**A**) A typical ultrasound image of a vein in the dorsum of the hand. (**B** and **C**) Time-resolved detection of PA signals from a vein against the background of pigmented skin and deep vessels in a healthy volunteer (B) and a patient (C). (**D** to **G**) Examples of PA traces from a healthy volunteer (D and F) and a patient with melanoma (E and G) before (D and E) and after (F and G) signal processing including averaging. (**H**) Typical peaks in PA traces from patients with melanoma, showing two positive (single and multiple), one negative, and one mixed positive-negative PA contrast associated with single (left) and clustered (second) CTCs, a single white CBC (third), and CTC-CBC emboli (right), respectively.

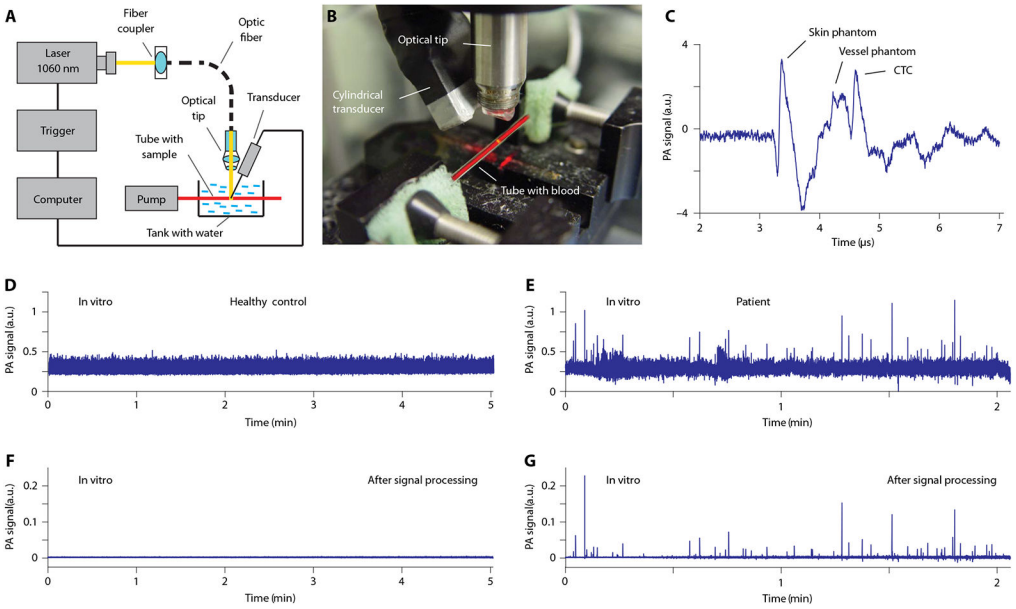

Fig. 3. In vitro PA detection of CTCs in blood samples from patients with melanoma.

(**A**) The schematic of in vitro PAFC with a vessel phantom consisting of a capillary tube and a focused cylindrical ultrasound transducer. Laser parameters: wavelength, 1060 nm; pulse width, 0.8 ns; pulse rate, 10 kHz; pulse energy, 50 μJ; linear beam size, 5 μm × 1 mm. Parameters of the customized ultrasound transducer: type, focused cylindrical; frequency, 32 MHz; focal length, 8 mm; lateral resolution, 65 μm. Both the capillary tube and transducer are located in a water tank. (**B**) Photo of the experimental setup used in vitro without the skin phantom (chicken skin) (28). (**C**) Typical PA signal from a single CTC in blood. (**D** to **G**) (D) and (F) show PA traces from unprocessed blood samples for healthy volunteers, whereas (E) and (G) show the same for patients with melanoma before (D and E) and after (F and G) signal processing.

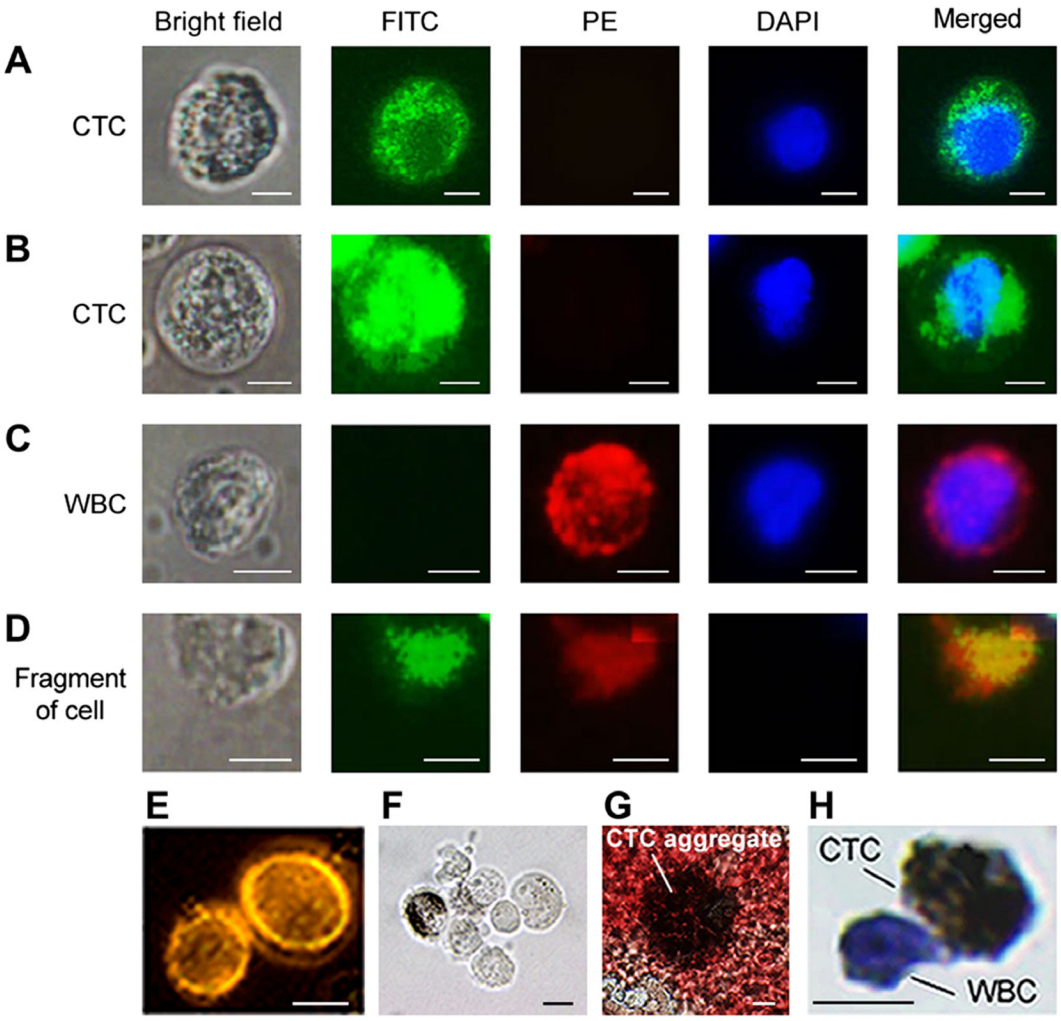

Fig. 4. Bright field and fluorescence images of cells from patient blood samples stained with dyes and targeted by antibodies.

(**A** and **B**) Nucleated (DAPI, blue) melanoma CTCs that express MCSP and CD146 receptors targeted by antibodies conjugated with FITC (green). A CTC with higher melanin content (A) exhibits lower fluorescence intensity compared to a CTC with lower melanin content (B). (**C**) A WBC that expresses the CD45 receptor, targeted by an antibody conjugated to PE dye (red). It does not have the MCSP and CD146 melanoma markers (no FITC fluorescence) and has a nucleus identified by DAPI (blue). (**D**) Debris that took up dyes nonspecifically and has no nucleus (no blue color). (**E** to **G**) Examples of CTC clusters consisting of two (E), seven (F) (bright field image), and many (≥20) CTCs, which are partly damaged and have released melanin (G). (**H**) An immunocytochemically stained single CTC (brown) with attached WBC (blue). Scale bars, 5 μm (A to D) and 10 μm (E to H).

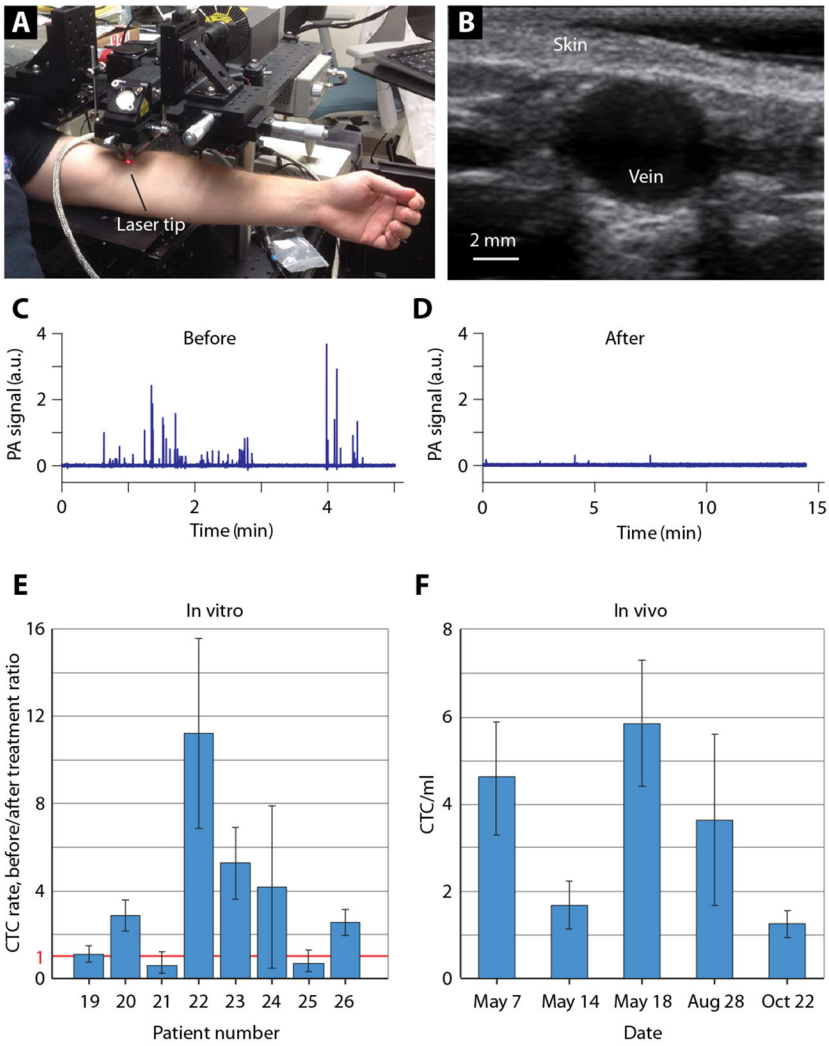

Fig. 5. Laser-based CTC theranostics directly in the patient's bloodstream.

(**A**) Photo of experimental setup for laser exposure of the cubital vein. (**B**) Typical ultrasound image of the relatively large cubital vein. In vivo PA signal traces before (**C**) and after (**D**) laser exposure of the cubital vein (diameter, 3.3 mm; depth, 1.6 mm; flow velocity, 7.5 cm/s) during 1-hour laser exposure. Laser parameters: wavelength, 1060 nm; pulse width, 5 ns; pulse rate, 1 kHz; pulse energy 240 μJ; linear beam size, 30 μm × 2.8 mm. (**E**) Ratios of CTC rates in several patients before and after laser theranostics in vitro in a glass tube with a diameter of 0.8 mm and flow velocity of 1 cm/s. (**F**) Monitoring of CTC rate in a patient with melanoma over 6 months.

Table 1.
Detection of CTCs in melanoma patients with PAFC in vivo.

For P1 to P15: CTCs per milliliter in vivo versus in vitro, Spearman correlation = +0.570 (P = 0.0266); CTC patient result in vivo versus in vitro, concordance = 3 of 15 (20%) and Cohen's κ ± SE = 0.02 ± 0.13. For P19 to P28: CTCs per milliliter in vivo versus in vitro, Spearman correlation = +0.527 (P = 0.1172); CTC patient result in vivo versus in vitro, concordance = 2 of 10 (20%) and Cohen's κ ± SE = 0.00 ± 0.16.

CTCs	In vivo PAFC			
Subject no.	Blood volume*	Number detected	CTCs per milliliter†	Patient result‡
P1	234	276	1.178 ± 0.071	Yes
P2	117	238	2.033 ± 0.132	Yes
P3	842	120	0.143 ± 0.013	Yes
P4	690	32	0.046 ± 0.008	Yes
P5	150	0	0.000 ± 0.000	No
P6	501	3	0.006 ± 0.003	Yes
P7	667	15	0.022 ± 0.006	Yes
P8	954	72	0.075 ± 0.009	Yes
P9	658	43	0.065 ± 0.010	Yes
P10	509	51	0.100 ± 0.014	Yes
P11	164	5	0.030 ± 0.014	Yes
P12	200	77	0.385 ± 0.044	Yes
P13	660	23	0.035 ± 0.007	Yes
P14	516	20	0.039 ± 0.009	Yes
P15	221	3	0.014 ± 0.008	Yes
P16	230	462	2.009 ± 0.093	Yes
P17	682	298	0.437 ± 0.025	Yes
P18	235	282	1.200 ± 0.071	Yes
P19	242	273	1.129 ± 0.068	Yes
P20	91	208	2.298 ± 0.159	Yes
P21	197	11	0.056 ± 0.017	Yes
P22	295	171	0.580 ± 0.044	Yes
P23	174	219	1.257 ± 0.085	Yes
P24	301	63	0.210 ± 0.026	Yes
P25	33	49	1.472 ± 0.210	Yes
P26	163	52	0.319 ± 0.044	Yes
P27	266	15	0.056 ± 0.015	Yes
P28	80	22	0.274 ± 0.058	Yes

*Blood volume is in milliliters.

†Point estimate ± SE of the estimate.

‡Patient result was calculated as "yes" if the patient's CTC rate (in CTCs per milliliter) was elevated above the false-positive CTC rate by >2 SEs of the difference. False-positive CTC rates ± SEs were 0.0040 ± 0.0008 CTCs/ml in vivo and 0.465 ± 0.147 CTCs/ml in vitro.

Table 2.
Detection of CBCs in melanoma patients with PAFC in vivo.

For P1 to P15: CBCs per milliliter in vivo versus in vitro, Spearman correlation = +0.024 (P = 0.93); CBC patient result in vivo versus in vitro, concordance = 12 of 15 (80%) and Cohen's κ ± SE = −0.10 ± 057. For P19 to P28: CTCs per milliliter in vivo versus in vitro, Spearman correlation = +0.450 (P = 0.1921); CTC patient result in vivo versus in vitro, concordance = 10 of 10 (100%).

CBCs	In vivo PAFC			
Subject no.	Blood volume*	Number detected	CBCs per millilite†	Patient result‡
P1	234	1	0.004 ± 0.004	Yes
P2	117	0	0.000 ± 0.000	No
P3	842	0	0.000 ± 0.000	No
P4	690	9	0.013 ± 0.004	Yes
P5	150	0	0.000 ± 0.000	No
P6	501	1	0.008 ± 0.002	Yes
P7	667	0	0.000 ± 0.000	No
P8	954	1	0.001 ± 0.001	No
P9	658	0	0.000 ± 0.000	No
P10	509	0	0.000 ± 0.000	No
P11	164	0	0.000 ± 0.000	No
P12	200	0	0.000 ± 0.000	No
P13	660	0	0.000 ± 0.000	No
P14	516	0	0.000 ± 0.000	No
P15	221	0	0.000 ± 0.000	No
P16	230	9	0.039 ± 0.013	Yes
P17	682	0	0.000 ± 0.000	No
P18	235	0	0.000 ± 0.000	No
P19	242	0	0.000 ± 0.000	No
P20	91	0	0.000 ± 0.000	No
P21	197	0	0.000 ± 0.000	No
P22	295	0	0.000 ± 0.000	No
P23	174	0	0.000 ± 0.000	No
P24	301	0	0.000 ± 0.000	No
P25	33	0	0.000 ± 0.000	No
P26	163	0	0.000 ± 0.000	No
P27	266	0	0.000 ± 0.000	No
P28	80	0	0.000 ± 0.000	No

*Blood volume is in milliliters.

†Point estimate ± SE of the estimate.

‡Patient result was calculated as "yes" if the patient's CBC rate {in CBCs per milliliter) was elevated above the false-positive CBC rate by >2 SEs of the difference. False-positive CBC rates ± SEs were 0.000 ± 0.000 CBCs/ml in vivo and 0.372 ± 0.131 CBCs/ml in vitro.